Bistability and field-induced transparency in superconducting quantum interference devices

Amitabh Joshi* and Min Xiao†
Department of Physics, University of Arkansas, Fayetteville, Arkansas 72701, USA
(Received 21 February 2007; published 2 January 2008)

The bistable behavior and field induced transparency are demonstrated in a quantum-mechanical treatment of coherently driven superconducting quantum interference devices having cubic nonlinearity in the polarizability.

DOI: 10.1103/PhysRevB.77.024502 PACS number(s): 85.25.−j, 42.65.Pc, 42.50.Gy

In recent years there have been many increasing activities for quantum information processing and quantum computing.[1] Among the many methodologies for quantum computing, superconducting devices including Cooper pair boxes, Josephson junctions, and superconducting quantum interference devices (SQUIDs) (Refs. 2–10) have shown great potential in realizing quantum gates and implementing quantum information processing. Such systems have great advantage in terms of easy fabrication and relatively long decoherence time thus potentially suit for large scale quantum computing.[11–13] For SQUID systems, demonstration of macroscopic quantum phenomena,[3] population inversion between low-lying levels,[4] and coherent manipulation of quantum states[11] are reported.

The applicability of the laws of quantum mechanics to macroscopic degrees of freedom was considered nearly 30 years ago[14] and that pushed the development of superconducting junction circuits displaying quantum behavior at the level of their macroscopic electrical variables. In fact, it was the pioneering work of Widmom[14] that raised the possibility of large scale quantum effects in superconducting devices. Such devices are characterized by quantized flux and/or charge states depending on their fabrication parameters. Rabi oscillation, Ramsey interferometry, and other spectroscopy experiments, have revealed that superconductive quantum devices behave as artificial atoms having quantized energy levels under controlled conditions.[2,6,7,11–13] The initial efforts for studying quantum tunneling paths in superconducting weak links were made in the early 1980's.[15] Experimental work on macroscopic quantum tunneling[16] and quantum-mechanical phase locking in arrays of Josephson junction was also demonstrated.[17] Here we study atomic analogue of such devices for other quantum optical effects associated with atoms, i.e., the bistable behavior and field induced transparency.[18–20] We carry out quantum treatment of a coherently driven (which we call here by probe and control fields) SQUID including cubic nonlinearity in the polarizability to demonstrate bistability and RF field-induced transparency. Such field-induced transparency is very suitable to control absorptive, dispersive properties of SQUIDs, and the bistable behavior so obtained has potential to realize memories[21] using these devices.

The SQUID considered here consists of Josephson tunnel junction enclosed by a circular superconducting loop, which is coupled through a constant static external flux Φ_{ex}, operating at low temperature T. The Hamiltonian for the SQUID with junction capacitance C and loop inductance L can be described as

$$H = \frac{Q^2}{2C} + \hbar\nu[1 - \cos(2\pi\Phi/\Phi_0)] + \frac{(\Phi - \Phi_{ex})^2}{2L}, \quad (1)$$

where Φ (the magnetic flux threading the loop) and Q (the total charge on the capacitor) are the conjugate variables of the system (satisfying the commutation relation $[\Phi, Q] = i\hbar$),[14] $\hbar\nu/2$ is the matrix element for the Josephson tunneling through the weak link (with critical current $I_c = 2e\nu$), $\Phi_0 = h/2e$ is the superconducting flux quantum. We can rewrite the Hamiltonian of Eq. (1) by expanding the "cosine" term as

$$H = \frac{Q^2}{2C} + \frac{C}{2}\omega_0^2\Phi^2 - \frac{\Phi\Phi_{ex}}{L} + H^R, \quad (2)$$

in which $\omega_0^2 = \left(\frac{1}{CL} + \frac{4\pi^2\hbar^2\nu}{C\Phi_0^2}\right)$, and H^R contains all other higher-order terms in Φ^2:

$$H^R = -\frac{2}{3}\hbar\nu(\pi\Phi/\Phi_0)^4 + \frac{4}{45}\hbar\nu(\pi\Phi/\Phi_0)^6 - \cdots. \quad (3)$$

Q and Φ can be expressed in terms of annihilation (creation) operator $a(a^\dagger)$ as

$$Q = i\sqrt{\frac{\hbar\omega_0 C}{2}}(a - a^\dagger), \quad \Phi = \sqrt{\frac{\hbar}{2\omega_0 C}}(a^\dagger + a). \quad (4)$$

With the substitution of Eq. (4) in Eq. (2) we obtain

$$H = \hbar\omega_0 a^\dagger a + \hbar\xi(a + a^\dagger) + H^R, \quad (5)$$

where $\xi = \Phi_{ex}/\sqrt{(2\hbar\omega_0 CL^2)}$.

The SQUID is inductively coupled to the rf field via the interaction Hamiltonian[22]

$$H_{int}^m = \lambda_m(\Phi - \Phi_{ex})\Phi_m, \quad (6)$$

in which λ_m is the coupling coefficient between the SQUID and the rf field specified by parameter m. Φ_m is the magnetic flux generated by the magnetic component of the rf field m and is given by $\Phi_m = \int_s \vec{B}_m(t)d\vec{s}$, where s is any surface that is bounded by the ring. $\vec{B}_m(t) = \vec{B}_m(0)\cos(\omega_m t + \theta_m)$ with $\vec{B}_m(0)$, ω_m, θ_m being amplitude, frequency, and phase of the rf field m, respectively.

We allow the interaction of SQUID with two rf fields of frequencies ω_1 and ω_2, respectively, so the total Hamiltonian becomes

$$H^T = \hbar\omega_0 a^\dagger a + \hbar\xi(a + a^\dagger) + \hbar g_1(a^\dagger e^{-i\omega_1 t} + a e^{i\omega_1 t}) + \hbar g_2(a^\dagger e^{-i\omega_2 t} + a e^{i\omega_2 t}) + H^R. \quad (7)$$

Here g_1 and g_2 are Rabi frequencies associated with the probe and control fields, respectively, and defined as $g_m = |\frac{\lambda m}{2\hbar}\langle i|\Phi|j\rangle|\Phi'_m$ with $\Phi'_m = \int_s \vec{B}_m(0)d\vec{s}$ $(m=1,2)$.

When θ is small, we approximate $H^R \cong -\frac{2}{3}\hbar\nu(\pi\Phi/\Phi_0)^4$. We then work in a frame rotating with the frequency (ω_2) of control field and omit rapidly oscillating terms to obtain

$$H^{\mathrm{TR}} = \hbar\Delta a^\dagger a + \hbar\alpha a^{\dagger 2}a^2 + \hbar g_1(a^\dagger e^{-i\delta t} + a e^{i\delta t}) + \hbar g_2(a^\dagger + a), \quad (8)$$

where $\Delta = \omega_0 - \omega_2 - \alpha$, $\delta = \omega_1 - \omega_2$, and $\alpha = \nu\left(\frac{\hbar\pi}{\Phi_0\sqrt{\omega_0 C}}\right)^4$.

With the currently available microfabrication techniques it is possible to choose the parameters $C \sim 10^{-12}$ F, $L \sim 10^{-10}$ H, $\hbar\nu(=0.047\Phi_0^2/L)$, $\omega_0/2\pi = 100$ GHz, and hence $\nu/\omega_0 \sim 10$. The critical current is of the order of $I_C = 6\mu A$. For a superconducting standing-wave cavity and SQUID located at one of the antinodes of the B field, the coupling constant is $g \sim 10^8$ s^{-1}. In terms of this coupling constant one can estimate other parameters $\xi/g \cong 10$, $\alpha/g \cong 5\times 10^{-2}$ and hence the device gives rise to a strong nonlinearity. The coefficient (or the strength parameter) β of next higher-order nonlinearity is estimated to be $\beta/g \cong 10^{-5}$ and thus we neglect such term in this work. Reported dephasing times are of the orders of hundreds of nanoseconds which makes the device less sensitive to external flux and its noises.[11] The coupling parameters depend on the frequency, but for the sake of simplicity of analysis we keep them as constants as the values of δ and Δ are kept small in comparison to ω_0.

The Heisenberg equation of motion for the system is given by

$$\dot{a} = -i\Delta a - 2i\alpha a^\dagger a^2 - ig_1 e^{-i\delta t} - ig_2. \quad (9)$$

Though we work at low temperature but still some normal damping will be present. We can rewrite the above equation including the damping term (in the limit of $T \to 0$) as

$$\dot{a} = -(i\Delta + \gamma)a - 2i\alpha a^\dagger a^2 - ig_1 e^{-i\delta t} - ig_2, \quad (10)$$

where γ is related to the linewidth of the associated SQUID transition. In order to solve Eq. (10), we use following ansatz:[23]

$$a(t) \cong a^{(0)} + a^{(1)}e^{-i\delta t} + a^{(-1)}e^{i\delta t}, \quad (11)$$

and do not consider any quantum correlations.[24] If the quantum fluctuations are not considered then the classical-type solution is the simplest solution of the problem, however, still rich in information to predict bistability and estimation of susceptibilities as we will see in the following. We get

$$ig_2 = (i\Delta + \gamma)a^{(0)} + 2i\alpha|a^{(0)}|^2 a^{(0)} + 2i\alpha[2a^{(0)}(|a^{(1)}|^2 + |a^{(-1)}|^2) + 2a^{(0)}a^{(1)}a^{(-1)}],$$

$$i\delta a^{(1)} = (i\Delta + \gamma)a^{(1)} - ig_1 + 4i\alpha|a^{(0)}|^2 a^{(1)} + 2i\alpha[(a^{(0)})^2(a^{(-1)})^* + |a^{(1)}|^2 a^{(1)}],$$

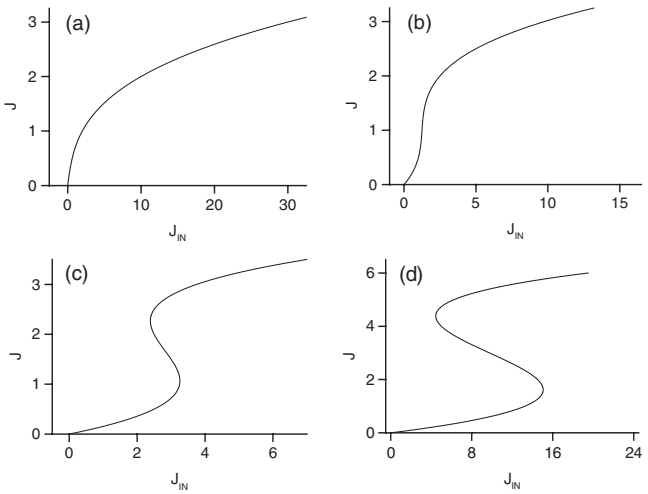

FIG. 1. Plot of J (arbitrary units) as a function of J_{IN} (arbitrary units) for different values of parameter Δ/γ. Curves (a), (b), (c), and (d) are for $\Delta/\gamma = 0.0, -1.5, -2.5$, and 4.5, respectively. Here J_{IN} is measured in $2\alpha/\gamma^3$ (which is also applicable for all the plots) and it corresponds to magnetic field strengths in the range of several nanotesla.

$$-i\delta a^{(-1)} = (i\Delta + \gamma)a^{(-1)} + 4i\alpha|a^{(0)}|^2 a^{(-1)} + 2i\alpha[(a^{(0)})^2(a^{(1)})^* + |a^{(-1)}|^2 a^{(-1)}]. \quad (12)$$

Since $a^{(\pm 1)} < a^{(0)}$ so we can neglect terms such as $a^{(0)}(a^{(\pm 1)})^2$, $(a^{(\pm 1)})^2 a^{(\pm 1)}$ in the subsequent discussions and obtain solutions for $a^{(0)}$ and $a^{(1)}$ as

$$a^{(0)} = i\frac{(g_2/\gamma)}{1 + i[\Delta/\gamma + (2\alpha/\gamma)|a^{(0)}|^2]}, \quad (13)$$

$$a^{(1)} = \frac{i(g_1/\gamma)[1 - i(\delta/\gamma + \Delta/\gamma + 4(\alpha/\gamma)|a^0|^2)]}{\{(i\delta/\gamma - 1)^2 + [\Delta/\gamma + 4(\alpha/\gamma)(|a^0|)^2]^2 - 4(\alpha/\gamma)^2(a^0)^4\}}. \quad (14)$$

Using Eq. (13) we can get the following relationship between the intensity of field $(J = |a_0|^2)$ threading the loop and the input driving field intensity $[J_{\mathrm{IN}} \sim (g_2)^2]$ as

$$J_{\mathrm{IN}} = [\gamma^2 + (\Delta + 2\alpha J)^2]J. \quad (15)$$

Equation (15) exhibits bistability. The turning points corresponding to upper and lower thresholds of the hysteresis cycle are given by $J^{U,L} = -\frac{2\Delta}{6\alpha} \pm \frac{\sqrt{(\Delta^2 - 3\gamma^2)}}{6\alpha}$.

According to Hurwitz criterion[24] one finds stable branches for $J > J^U$ and $J < J^L$ but if the value of J is in between these threshold values then there is an unstable branch. So, the above state equation predicts bistability under the condition $\Delta^2 > 3\gamma^2$ provided the signs of Δ and α are opposite, i.e., $\Delta.\alpha < 0$. In Fig. 1 we plot the curves for J vs J_{IN} under different values of Δ. Curves (a), (b), (c), and (d) are for $\Delta/\gamma = 0, -1.5, -2.5$, and -4.5, respectively. It is clear that there is no bistability for lower values of Δ, i.e., $\Delta^2 < 3\gamma^2$. In curve (c) bistability starts to appear as the condition $\Delta^2 > 3\gamma^2$ is satisfied. With further increase in Δ value, the prominent hysteresis curve of bistability is apparent in

curve (d). Both deterministic as well as stochastic (noise-induced) switching is possible in this system. We have to use alternate triggering of up and down controlling rf pulses for demonstrating the deterministic switching and storage ability of the SQUID system similar to the atomic system.[21] Also, it may be possible to use certain designs of SQUIDs, which are not sensitive to the noise[11] so the deterministic switching is prominent. We give some parameters for the experimental consideration. SQUIDs can be fabricated using planer components with lateral dimensions $\sim 10\ \mu$m, giving values of L, C, $\omega_0/2\pi$, and Z_0 (the characteristic impedance) as $\sim 10^{-10}$ H, 10^{-12} F, 100 GHz, and 10 Ohms, respectively. If aluminium is used then a good BCS superconductor with transition temperature of 1.1 K and a gap of 200μ V can be obtained. Typical damping parameter (γ) for SQUIDs is of the order of 3×10^6 Hz and the Δ values depicted in Fig. 1 is in the range 0–15 MHz, much less than ω_0. A typical Rabi frequency for the SQUIDs is about 10^8 Hz, which implies that the magnetic field strength of several nanotesla or more is required in such observations. For observing such a bistable behavior we do not require two driving fields. Such behavior can be observed with a single driving field.[18,19] We have given here a general formulation of the problem by considering two driving fields to demonstrate the controllability of the probe susceptibility with control field, which will be discussed next.

We can explore absorptive and dispersive characteristics of this SQUID by studying imaginary and real parts of the susceptibility with respect to the probe field

$$\mathrm{Re}[\chi] \propto -\frac{\gamma(\delta+\Delta+2J)(\Delta^2+4\Delta J+3J^2+1-\delta^2+2\delta)}{[(\Delta+J)(\Delta+3J)]^2+[1+\delta^2]^2+2[(\Delta+J)(\Delta+3J)(1-\delta^2)]}, \tag{16}$$

$$\mathrm{Im}[\chi] \propto -\frac{\gamma[(\Delta-\delta+2J)^2+(1-J^2-4\delta^2)]}{[(\Delta+J)(\Delta+3J)]^2+[1+\delta^2]^2+2[(\Delta+J)(\Delta+3J)(1-\delta^2)]}. \tag{17}$$

In the above expressions the explicit appearance of control field is with its frequency detuning Δ. The values of Δ's are in the range from 0 to ± 90 MHz and that of δ are in the range from 0 to tens of MHz. The intensity of the control field is implicitly appearing due to the parameter J. The control field intensity J_{IN} and J are related via Eq. (15) which determines J for a given J_{IN}. So, any change in control field intensity is reflected in J. We have absorbed factor α in J and J_{IN} in the above expressions. J_{IN} is measured in $2\alpha/\gamma^3$ and it corresponds to magnetic field strengths in the range of several nanotesla. We plot these expressions of Im[χ] and Re[χ] in Figs. 2–5 with respect to the control field's frequency detuning (Δ). Hence the probe susceptibility with respect to Δ may give rise to some unusual and interesting results. In Figs. 2 and 3 we plot Im[χ] and Re[χ], respectively, for different J values under the condition $\delta/\gamma=1$ for all the curves. Curves (a), (b), (c), and (d) are for $J=0$, 1.5, 2.35, and 7.0, respectively. Curve (a) displays usual absorptionlike (dispersionlike) profile in Fig. 2 (Fig. 3) because of the small value of J here. As J is increased to $J=1.5$, the absorption

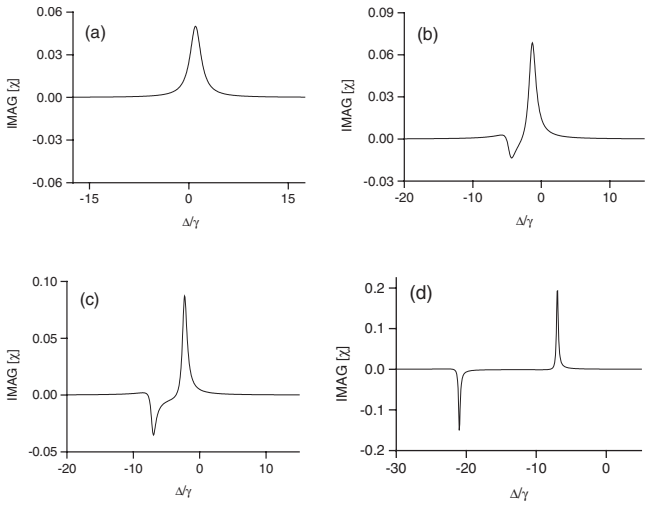

FIG. 2. Imaginary part of susceptibility (dimensionless and scaled) as a function of Δ/γ (dimensionless) under the condition $\delta/\gamma=1.0$. Curves (a), (b), (c), and (d) are for $J=0.0$, 1.5, 2.35, and 7.0, respectively.

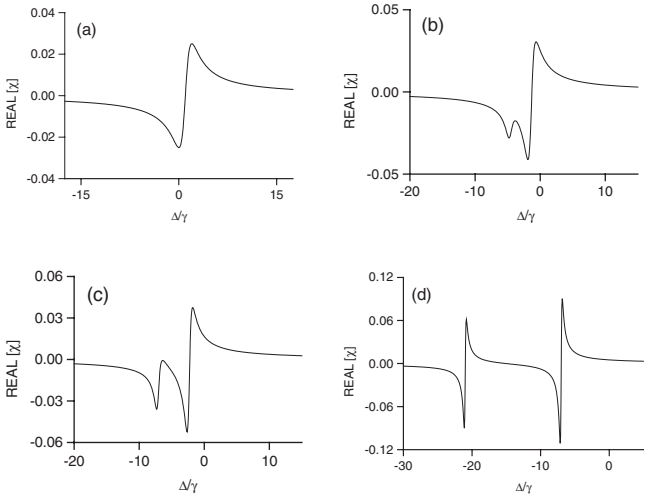

FIG. 3. Real part of susceptibility (dimensionless and scaled) as a function of Δ/γ with other conditions as in Fig. 2.

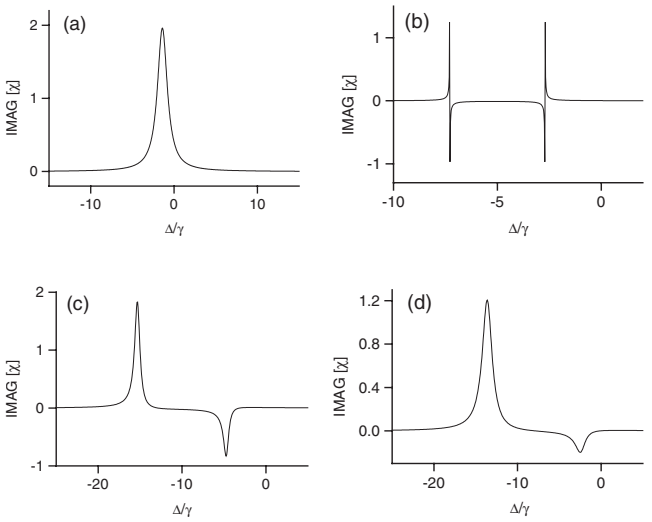

FIG. 4. Imaginary part of susceptibility as a function of Δ/γ. Curves (a), (b), (c), and (d) are for $(\delta/\gamma, J)=(0.0, 0.7)$, (0.0, 2.5), $(-2.0, 5.0)$, and $(-4.0, 4.0)$, respectively.

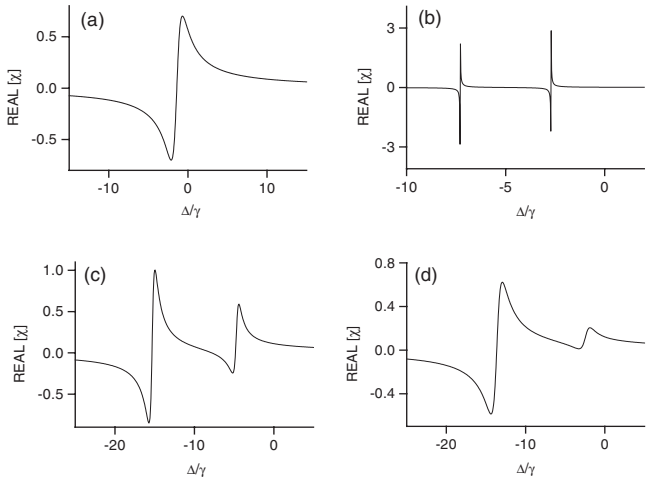

FIG. 5. Real part of susceptibility as a function of Δ/γ with other conditions as in Fig. 4.

profile changes to a dispersionlike profile for Im[χ] [Fig. 2(b)] but for Re[χ] the lower part of the dispersionlike profile splits into two parts [Fig. 3(b)]. Further increase of J (=2.35) clearly shows two peaks in Im[χ] with one corresponding to absorptionlike and another inverted-absorption-like (Fig. 2(c)). Also, there is a width narrowing feature under this condition. Correspondingly in Re[χ] the splitting of lower profile looks more prominent [Fig. 3(c)]. For even larger value of J (=7), the narrowed absorptionlike and inverted-absorption-like profiles approach towards equal magnitudes and their separation increases considerably [Fig. 2(d)]. Interestingly for this value of J, we find that Re[χ] also displays two clear cut dispersionlike features very much separated with each other [Fig. 3(d)]. By examining Figs. 2(a)–2(d), it is clear that as J increases, there is transparency in the system around $\Delta/\gamma=0$ introduced by driving field. Also, for large J value there is another region of transparency between the two peaks (one showing absorption and another gain) as evident from Fig. 2(d).

The singularities of real and imaginary parts of the susceptibility are determined by $\Delta=-2J\pm\sqrt{J^2-1+\delta^2+2i\delta}$, which locate two peaks appearing in Figs. 2(d) and 3(d) very easily. Further interesting results for real and imaginary parts of the susceptibility are presented in Figs. 4 and 5, respectively. Curves (a) and (b) of Figs. 4 and 5 are for $(\delta/\gamma=0, J=0.7)$ and $(\delta/\gamma=0, J=2.5)$, respectively. Curve (a) of Fig. 4 (Fig. 5) shows absorptionlike profile shifted towards negative Δ value. When J is increased to $J=2.5$, there is a dramatic change in the profiles of Im[χ] [Fig. 4(b)] and Re[χ] [Fig. 5(b)]. The structure of Im[χ] now splits into two peaks having dispersionlike profiles and the Re[χ] also shows two narrowed dispersionlike profiles. The slope of Re[χ] is very steep with respect to Δ which can provide slow light propagation in this case giving rise to all important effects of such slow fields in SQUID device. Effects of negative value of δ on Im[χ] and Re[χ] are presented in Figs. 4(c) and 4(d) and Figs. 5(c) and 5(d), respectively. Curves (c) and (d) in Figs. 4 and 5 are for $\delta/\gamma=-2$, $J=5$ and $\delta/\gamma=-4$, $J=4$, respectively. Clearly, both J and δ/γ compete with each other to determine the profiles of the two peaks under these conditions. The Im[χ] in Figs. 4(c) and 4(d) exhibit double peaks having absorptionlike and inverted-absorption-like profiles. If J is more than δ/γ [curve (c)] then there is narrowing in these peaks. The Re[χ] also gives two dispersionlike profiles in curves (c) and (d) of Fig. 5. From curves (a)–(d) of Fig. 4, we find that field-induced transparency increases at $\Delta/\gamma=0$ as the field magnitude is increased in these curves. The refractive and absorptive susceptibilities get enhanced due to the nonlinearity and provide effects such as field-induced transparency useful in quantum-information processing. So, the phenomenon of field-induced-transparency observed in atomic molecular media can be observed in solid state system of SQUIDs. The physical mechanism involved is the presence of control field (causing dynamic stark-splitting-like effect) and the nonlinearity.

In summary, studies of SQUID characterized by quantized flux and/or charge states with driving fields are presented here which shows controllability of its susceptibility with control field giving rise to transparency. Such device also exhibits bistable characteristics under certain parametric conditions which can be used as memory elements in circuit cavity quantum electrodynamic systems. It is also possible to produce Schrödinger cat state using third order nonlinearity offered by this device.

We acknowledge the funding support from the National Science Foundation.

*ajoshi@uark.edu
†mxiao@uark.edu

[1] M. A. Nielsen and I. L. Chuang, *Quantum Computation and Quantum Information* (Cambridge Univesity Press, Cambridge, 2001).
[2] J. M. Martinis and R. L. Kautz, Phys. Rev. Lett. **63**, 1507 (1989).
[3] R. Rouse, S. Han, and J. E. Lukens, Phys. Rev. Lett. **75**, 1614 (1995).
[4] S. Han, R. Rouse, and J. E. Lukens, Phys. Rev. Lett. **76**, 3404 (1996).
[5] Y. Makhlin, G. Schoen, and A. Shnirman, Nature (London) **398**, 305 (1999).
[6] Y. Nakamura, Y. Pashkin, and J. S. Tsai, Nature (London) **398**, 786 (1999).
[7] C. H. van der Wal, A. C. J. ter Haar, F. K. Wilhelm, R. N. Schouten, C. J. P. M. Harmans, T. P. Orlando, S. Lloyd, and J. E. Mooij, Science **290**, 773 (2000).
[8] J. R. Friedman, V. Patel, W. Chen, S. K. Tolpygo, and J. E. Lukens, Nature (London) **406**, 43 (2000).
[9] A. Steinbach, P. Joyez, A Cottet, D. Esteve, M. H. Devoret, M. E. Huber, and J. M. Martinis, Phys. Rev. Lett. **87**, 137003 (2001).
[10] W. Xiang-bin and M. Keiji, Phys. Rev. B **65**, 172508 (2002).
[11] D. Vion, A. Aassime, A. Cottet, P. Joyez, H. Pothier, C. Urbina, D. Esteve, and M. H. Devoret, Science **296**, 886 (2002).
[12] Y. Yu, S. Han, X. Chu, S. I. Chu, and Z. Wang, Science **296**, 889 (2002).
[13] I. Chiorescu, Y. Nakamura, C. J. P. M. Harmans, and J. E. Mooij, Science **299**, 1869 (2003).
[14] See, for example, A. Widom, J. Low Temp. Phys. **37**, 449 (1979) who was first to discuss the possiblity of constructing macroscopic superconducting circuits exhibiting quantum behavior and also proposed magnetic flux (Φ) and charge (Q) commutator bracket; A. J. Leggett and A. Garg, Phys. Rev. Lett. **54**, 857 (1985).
[15] T. D. Clark and A. Widom, Phys. Rev. Lett. **46**, 1704 (1981); Phys. Rev. B **30**, 1205 (1984).
[16] M. H. Devoret, J. M. Martinis, and J. Clarke, Phys. Rev. Lett. **55**, 1908 (1985); J. M. Martinis, M. H. Devoret, and J. Clarke, Phys. Rev. B **35**, 4682 (1987).
[17] A. Widom and C. Vittoria, Phys. Rev. B **44**, 12481 (1991).
[18] L. A. Lugiato, in *Progress in Optics*, edited by E. Wolf (North Holland, Amsterdam, 1984), Vol. 21, p. 71, and references therein.
[19] H. M. Gibbs, *Optical bistability: Controlling Light with Light* (Academic, New York, 1985), and references therein.
[20] A. Joshi and M. Xiao, *Progress in Optics*, edited by E. Wolf (North Holland, Amsterdam, 2006), Vol. 49, p. 97, and references therein.
[21] H. Chang, H. Wu, C. Xie, and H. Wang, Phys. Rev. Lett. **93**, 213901 (2004).
[22] C. P. Yang and S. Han, Phys. Lett. A **321**, 273 (2004); J. Zou and B. Shao, Phys. Lett. A **256**, 375 (1999).
[23] Y.-W. Jiang, K.-D. Zhu, Z.-J. Wu, X.-Z. Yuan, and M. Yao, J. Phys. B **39**, 2621 (2006); also see G. S. Agarwal, Phys. Rev. A **51**, R2711 (1995), where electromagnetic field induced transparency and bistability are discussed in high density exciton system.
[24] P. D. Drummond and D. F. Walls, J. Phys. A **13**, 725 (1980).